Experimental and DFT Studies of the Conversion of Ethanol and Acetic Acid on PtSn-Based Catalysts†

Rafael Alcala, John W. Shabaker, George W. Huber, Marco A. Sanchez-Castillo, and James A. Dumesic*

Department of Chemical Engineering, University of Wisconsin, Madison, Wisconsin 53706

Received: February 12, 2004; In Final Form: April 13, 2004

Reaction kinetics studies were conducted for the conversions of ethanol and acetic acid over silica-supported Pt and Pt/Sn catalysts at temperatures from 500 to 600 K. Addition of Sn to Pt catalysts inhibits the decomposition of ethanol to CO, CH_4, and C_2H_6, such that PtSn-based catalysts are active for dehydrogenation of ethanol to acetaldehyde. Furthermore, PtSn-based catalysts are selective for the conversion of acetic acid to ethanol, acetaldehyde, and ethyl acetate, whereas Pt catalysts lead mainly to decomposition products such as CH_4 and CO. These results are interpreted using density functional theory (DFT) calculations for various adsorbed species and transition states on Pt(111) and $Pt_3Sn(111)$ surfaces. The Pt_3Sn alloy slab was selected for DFT studies because results from in situ ^{119}Sn Mössbauer spectroscopy and CO adsorption microcalorimetry of silica-supported Pt/Sn catalysts indicate that Pt−Sn alloy is the major phase present. Accordingly, results from DFT calculations show that transition-state energies for C−O and C−C bond cleavage in ethanol-derived species increase by 25−60 kJ/mol on $Pt_3Sn(111)$ compared to Pt(111), whereas energies of transition states for dehydrogenation reactions increase by only 5−10 kJ/mol. Results from DFT calculations show that transition-state energies for CH_3CO−OH bond cleavage increase by only 12 kJ/mol on $Pt_3Sn(111)$ compared to Pt(111). The suppression of C−C bond cleavage in ethanol and acetic acid upon addition of Sn to Pt is also confirmed by microcalorimetric and infrared spectroscopic measurements at 300 K of the interactions of ethanol and acetic acid with Pt and PtSn on a silica support that had been silylated to remove silanol groups.

Introduction

The selective conversion of oxygenated hydrocarbons is important for various chemical processes, such as the production of chemicals from renewable resources. For example, it is desirable to selectively reduce organic acid groups to hydroxyl groups, such as in the conversion of lactic acid to propylene glycol.[1−4] In addition, it is desirable to selectively oxidize alcohols to aldehydes or ketones,[5−12] while limiting the cracking of reactants to form CO and light alkanes. In this respect, addition of Sn to Pt catalysts typically inhibits cracking reactions involving cleavage of C−C bonds, and PtSn-based catalysts are more resistant to coking compared to Pt catalysts.[13−16] The inhibition of C−C bond cleavage reactions by addition of Sn to Pt catalysts has been attributed to changes in the geometric and electronic nature of the surface. For example, Sn may decrease the size of surface Pt ensembles,[17,18] and hydrocarbon species may adsorb more weakly on PtSn catalysts compared to Pt catalysts.[19]

Results from density functional theory (DFT) calculations indicate that cleavage of C−C bonds in oxygenated hydrocarbons (e.g. ethanol) is more facile than C−C bond cleavage in alkanes (e.g. C_2H_6) on Pt(111).[20] Indeed, experimental studies show that ethanol reacts on Pt at 500 K to give CO, CH_4, and C_2H_6 by cleavage of C−O and C−C bonds.[21] Thus, it is necessary to inhibit these decomposition reactions if Pt-based catalysts are to be used for selective conversions of oxygenated hydrocarbons. In this respect, Sn may be a useful modifying agent. For example, it has been reported that addition of Sn to Ru inhibits cleavage of C−O and C−C bonds in oxygenated hydrocarbons.[22]

In the present paper, we present experimental results showing that addition of Sn to Pt catalysts inhibits the decomposition of ethanol to CO, CH_4, and C_2H_6, such that PtSn-based catalysts are selective for dehydrogenation of ethanol to acetaldehyde. In addition, we show that PtSn-based catalysts are selective for the conversion of acetic acid to ethanol, whereas Pt catalysts lead to the subsequent formation of products from ethanol decomposition (CO, CH_4, and C_2H_6). We also report results from microcalorimetric and infrared spectroscopic measurements to show that the presence of Sn inhibits cleavage of the C−C bond in ethanol and acetic acid over Pt-based catalysts. In situ ^{119}Sn Mössbauer spectroscopy and CO adsorption results indicate that the silica-supported PtSn catalysts used in this study are comprised mainly of a Pt−Sn alloy phase. Accordingly, we report results from DFT calculations employing $Pt_3Sn(111)$ slabs to interpret the observations from our experimental studies. In particular, we investigate adsorbed reaction intermediates and transition states for cleavage of C−C, C−O, C−H, and O−H bonds on $Pt_3Sn(111)$ slabs, and we compare the energies of these species with those on Pt(111). We show that the energies of transition states for C−C and C−O bond cleavage in C_2OH_x species derived from ethanol and acetic acid are higher on $Pt_3Sn(111)$ compared to Pt(111), whereas the energies of transition states for C−H and O−H bond cleavage, and the transition state for cleavage of the CH_3CO−OH bond in acetic acid, are increased by only small amounts upon addition of Sn.

† Part of the special issue "Michel Boudart Festschrift".

* To whom correspondence should be addressed. Phone: (608)262-1095. Fax: (608)262-5434. E-mail: dumesic@engr.wisc.edu. Corresponding author address: Department of Chemical Engineering, 1415 Engineering Drive, Madison, WI 53706.

10.1021/jp049354t CCC: $30.25
Published on Web 05/18/2004

Methods

Electronic structure calculations based on self-consistent, gradient-corrected density functional theory were conducted for two-layer $Pt_3Sn(111)$ slabs.[23] The 2×2 two-layer unit cell, containing 6 Pt atoms and 2 Sn atoms, was repeated periodically, with four equivalent layers of vacuum between any two successive metal slabs. Total energy calculations were performed using DACAPO.[24] Ionic cores are described by ultrasoft pseudopotentials,[25] and the Kohn−Sham one-electron valence states are expanded in a basis of plane waves with kinetic energies below 25 Ry. The surface Brillouin zone is sampled at 18 special k-points. The exchange-correlation energy and potential are described by the Perdew-Wang 1991 (PW91) generalized gradient approximation (GGA).[26,27] The self-consistent density is determined by iterative diagonalization of the Kohn−Sham Hamiltonian, Fermi-population of the Kohn−Sham states ($k_BT = 0.1$ eV), and Pulay mixing of the resulting electronic density.[28] All reported binding energies are calculated using the PW91 functional, and these energies have been extrapolated to $k_BT = 0$ eV.

Adsorption occurs on one side of the slab and all adsorbate atoms were allowed to relax, while the metal atoms are fixed in their bulk-terminated positions with a lattice constant of 4.00 Å.[29] Gas-phase calculations are carried out in a $15.00 \times 15.00 \times 15.75$ Å unit cell, and the Brillouin zone is sampled at one k-point. The magnetic moments of gas-phase radical species are optimized during the geometry optimizations. Transition states are estimated using constrained optimizations, where the bond length representing the reaction coordinate is constrained and all other degrees of freedom are optimized. The transition states are characterized by the configuration with the highest energy along the reaction coordinate and a transition from repulsive to attractive forces along the constrained bond.[29,30] This procedure for determining the transition state of relatively large adsorbates has proven to yield energy barriers of reasonable accuracy compared to more rigorous methods, such as the nudged elastic band method.[31−34]

All calculations were conducted on 2×2 unit cells, and convergence with respect to coverage was confirmed with calculations using a 3×3 unit cell. For example, the transition-state energies for acetic acid (CH_3CO-OH) dehydroxylation on 2×2 and 3×3 two-layer unit cells differ by only 13 kJ/mol. Note that in this study, acetic acid is the largest molecule investigated and is likely the most sensitive to coverage effects.

Experimental Section

(1) Catalyst Preparation. Silica-supported platinum catalysts were prepared by an ion-exchange technique for Mössbauer spectroscopy studies, CO microcalorimetric measurements, and reaction kinetics studies. An ion-exchange column filled with Amberlite IRA-400 resin was used to convert 300 mL of 0.010 M $Pt(NH_3)_4(NO_3)_2$ (tetraamine platinum nitrate) to 0.010 M $Pt(NH_3)_4(OH)_2$. In a separate beaker, the fumed silica was combined with 1 L of 0.001 M $Pt(NH_3)_4(NO_3)_2$ solution and stirred to form a slurry (pH = 3.4). The pH was then adjusted to 7.0 by dropwise addition of the 0.010 M $Pt(NH_3)_4(OH)_2$. After stirring for 2 h, the slurry was vacuum filtered and washed with 1.5 L of dilute NH_4OH solution (pH = 8.0) and then dried on the filter for 8 h. The filter cake was subsequently dried under air in an oven at 393 K overnight. Tin was added to the dried silica-supported Pt catalyst by evaporative deposition of tributyltin acetate dissolved in pentane. The pentane solution was added to the oven-dried catalysts, and the resulting slurry was stirred at room temperature until dry. After further drying in a hood overnight, the PtSn catalysts were calcined in flowing O_2 at 533 K for 4 h with a linear temperature ramp over 2 h. Metal loadings of 1.7 wt % Pt and 0.82 wt % Sn (for $PtSn_{0.8}/SiO_2$) or 4.4 wt % Sn (for $PtSn_4/SiO_2$) were determined by atomic absorption spectroscopy/inductively coupled plasma (AAS/ICP) after digestion in acids.

For microcalorimetric and FTIR studies of oxygenated hydrocarbons, capped silica-supported catalysts were prepared by chemical vapor deposition of platinum acetylacetonate (Aldrich) and tin acetate (Aldrich) precursors onto silica (Cab-O-Sil, Grade EH-5, Cabot Corporation). Platinum was deposited on the silica support at 473 K with a target Pt loading of 10 wt %. Tin was subsequently deposited on the silica-supported platinum for synthesis of the Pt−Sn alloy catalysts. The Sn deposition temperature was 473 K, and the desired Pt:Sn ratio of the Pt−Sn alloy catalysts was 1:1. Ethylene adsorption on Pt catalysts at 300 K confirmed the presence of large Pt ensembles through formation of ethylidyne surface species.[35] Ethylidyne surface species were not detected on Pt−Sn alloy catalysts, confirming the breakup of large Pt ensembles through alloying.

Prior to silylation, silica-supported catalysts were dehydroxylated in helium at 1173 K for 8 h with a 4 h ramp, and the metal surface was then saturated with CO at 300 K. The silica was silylated with trimethylethoxysilane (TMES) at 473 K for 12 h. Finally, CO was removed by oxidation with oxygen (Praxair) at 373 K for 1 h. The catalysts were reduced with hydrogen (AGA) at 373 K for 1 h and purged with helium (AGA) for 1 h at 373 K prior to use. Silylation is necessary because oxygenated hydrocarbons, such as ethanol, acetaldehyde, and acetic acid, are known to adsorb on untreated silica surfaces.[36] Adsorption on the support can dominate infrared spectra and microcalorimetric data collected for low metal loading catalysts.

(2) Mössbauer Spectroscopy. Mössbauer spectra were collected at 300 K with an Austin Science Associates Model S-600 Mössbauer spectrometer operated in constant-acceleration mode with a 20 mCi γ-ray $Ca^{119}SnO_3$ source. A 0.05 mm thick Pd foil was placed between the source and detector to filter 25.04- and 25.27-keV X-rays from the source. A $Xe-CO_2$ proportional counter was used for detection of the 23.88 keV γ-rays. Isomer shifts are reported relative to $CaSnO_3$ at 300 K. A glass cell with thin windows was used for treatments and to collect the Mössbauer data. The Pyrex cell was equipped with stopcocks that were closed to the atmosphere during data collection and opened for the various treatments. The Mössbauer spectroscopic data were fit to Lorentzian-type curves using the NLS package in R (R Foundation).

(3) Microcalorimetry and Infrared Spectroscopy Studies. The procedures for microcalorimetric and infrared spectroscopic studies have been described in detail elsewhere.[35] Briefly, microcalorimetric measurements were conducted at 300 K using a Setaram BT2.15D heat-flux calorimeter. The infrared spectroscopic studies were conducted using a Mattson spectrometer. All spectra were collected in the absorbance mode with 2 cm^{-1} resolution and 2500 scans.

(4) Reaction Kinetic Studies. Reaction kinetic studies of the conversion of acetic acid and ethanol in the presence of H_2 were conducted using a stainless steel apparatus and a Pyrex downflow reactor operating at 1 atm. Further details of the experimental procedure are given elsewhere.[37] The reactor feed consisted of 2.5 mol % acetic acid or ethanol, 80 mol % hydrogen, and helium as the balance. Catalysts were reduced in flowing H_2 by heating to 723 K over 8 h and holding at this

TABLE 1: ^{119}Sn Mössbauer Parameters of Pt−Sn Catalysts at 300 K[a]

sample and treatment	isomer shift (mm s^{-1})	quadrupole splitting (mm s^{-1})	width (mm s^{-1})	relative area (%)	chemical form of Sn
$PtSn_{0.8}/SiO_2$	1.93 (0.03)		1.79	79.9 (3.8)	Pt−Sn alloy
reduced at 723 K	0.36 (0.23)		0.62	2.3 (1.4)	Sn(IV)
	2.41 (0.10)	2.14 (0.22)	1.07	17.8 (4.0)	Sn(II)
$PtSn_{0.8}/SiO_2$	2.05 (0.02)		1.79	86.5 (1.2)	Pt−Sn alloy
treated with acetic acid + H_2 at 573 K	0.73 (0.04)		0.77	13.5 (1.2)	Sn(IV)
$PtSn_4/SiO_2$	2.03 (0.04)		1.80	67.8 (4.6)	Pt−Sn alloy
reduced at 723 K	0.59 (0.09)		0.72	4.6 (1.0)	Sn(IV)
	2.85 (0.03)	1.81 (0.07)	0.83	27.6 (4.7)	Sn(II)
$PtSn_4/SiO_2$	2.05 (0.04)		1.98	72.5 (1.8)	Pt−Sn alloy
treated with acetic acid + H_2 at 573 K	0.51 (0.03)		0.62	9.0 (0.6)	Sn(IV)
	3.00 (0.05)	1.76 (0.11)	0.95	18.5 (1.9)	Sn(II)

[a] Standard error is reported in parentheses, with constrained values for peak widths.

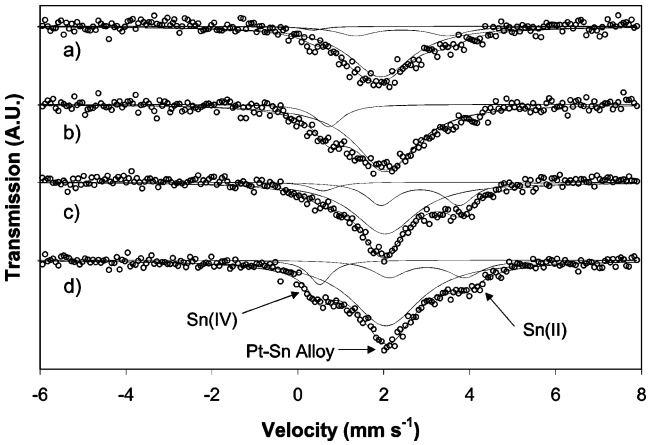

Figure 1. ^{119}Sn Mössbauer spectra of (a) $PtSn_{0.8}/SiO_2$ reduced in H_2 723 K, (b) $PtSn_{0.8}/SiO_2$ treated with acetic acid in H_2 at 573 K for 45 min, (c) $PtSn_4/SiO_2$ reduced in H_2 723 K, and (d) $PtSn_4/SiO_2$ treated with acetic acid in H_2 at 573 K for 45 min.

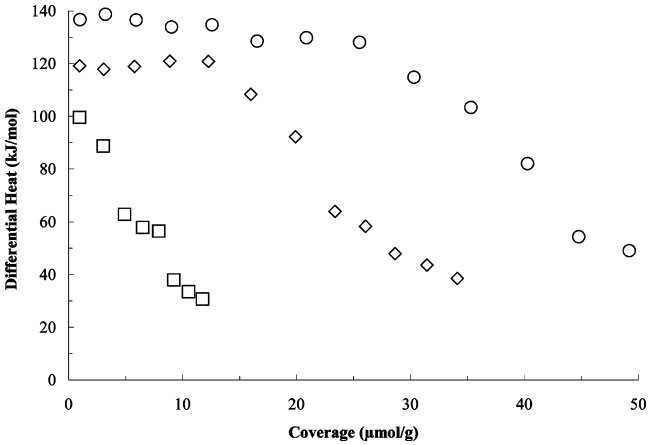

Figure 2. Differential heat of CO adsorption versus adsorbate coverage at 300 K for (○) Pt/SiO_2, (◇) $PtSn_{0.8}/SiO_2$, and (□) $PtSn_4/SiO_2$.

temperature for 2 h prior to collecting reaction kinetics data. Turnover frequencies are based on CO chemisorption uptakes of 45, 28, and 8 μmol/g for Pt/SiO_2, $PtSn_{0.8}/SiO_2$, and $PtSn_4/SiO_2$, respectively. The average reproducibility of these turnover frequencies was about 5−10% for major products (TOF > 500 h^{-1}) and 10−30% for minor products.

Results

(1) Characterization of Pt and PtSn Catalysts. *Mössbauer Spectroscopy.* Mössbauer spectra of the PtSn catalysts before and after reaction with acetic acid and H_2 are shown in Figure 1. Each spectrum was fit to three phases: a Pt−Sn alloy phase, a Sn(II) phase, and a Sn(IV) phase. The fitting parameters of these spectra are shown in Table 1. For the $PtSn_{0.8}/SiO_2$ and $PtSn_4/SiO_2$ catalysts, the major phase before and after reaction is the Pt−Sn alloy, accounting for over 67% of the area. Most of the ionic species of Sn (Sn(II) and Sn(IV)) are likely associated with the silica support. After exposure to the reaction mixture of acetic acid and H_2, the relative area of the Pt−Sn alloy species for the $PtSn_{0.8}/SiO_2$ catalyst changed from 80 (±4) to 87 (±1)%, the relative area of the Sn(IV) species increased from 2 (±1) to 14 (±1)%, and the relative area of the Sn(IV) species decreased from 18 (±4)% to essentially zero. When the $PtSn_4/SiO_2$ catalyst is exposed to reaction conditions, the relative area of the PtSn alloy changed from 68 (±5) to 73 (±2)%, the relative area of the Sn(IV) species increases from 5 (±1) to 9 (±1)%, and the relative area of the Sn(II) species decreases from 28 (±5) to 19 (±2)%. The change in relative area of the PtSn alloy before and after exposure to reactions conditions is within 2 times the standard error, indicating that this change is not statistically significant for both catalysts. These results are consistent with those of Margitfalvi et al., who used ^{119}Sn Mössbauer spectroscopy to observe the formation of a Sn(IV) species, a decrease in the Sn(II) species and no major change in the Pt−Sn alloy species for $Pt-Sn/SiO_2$ catalysts after reaction with crotonaldehyde and H_2 at 353 K.[38]

Microcalorimetry and Infrared Spectroscopy. Figure 2 shows plots of the differential heat of CO adsorption versus adsorbate coverage for the Pt/SiO_2, $PtSn_{0.8}/SiO_2$, and $PtSn_4/SiO_2$ catalysts. The initial heats of CO adsorption are equal to 137, 119, and 100 kJ/mol for these catalysts, respectively. These values are in good agreement with those of Shen et al. who reported that the initial heat of CO adsorption was 142 and 107 kJ/mol for Pt/SiO_2 and $PtSn_2/SiO_2$, respectively,[35] and the initial heat and the saturation coverage for adsorption of CO decreases with increasing tin content in the catalysts. These results provide strong evidence that essentially all of the Pt for these $PtSn/SiO_2$ samples has interacted with Sn to form PtSn alloys, otherwise the initial heat of CO adsorption would have been equal to the value characteristic of Pt (i.e., 142 kJ/mol).

Microcalorimetric and infrared spectroscopic studies for ethanol adsorption on capped silica-supported Pt and Pt−Sn catalysts were conducted at 300 K. The corresponding differential heats and spectra are shown in Figures 3 and 4. The initial heat for ethanol interaction with silica-supported Pt is 95 kJ/mol (Figure 3A, solid square symbols). During these measurements, gas evolution (e.g., H_2) was observed from ethanol decomposition (dehydrogenation and C−C bond cleavage). Infrared spectroscopy bands were observed at 2060 and 1850 cm^{-1}, corresponding to adsorbed atop and bridge-bonded

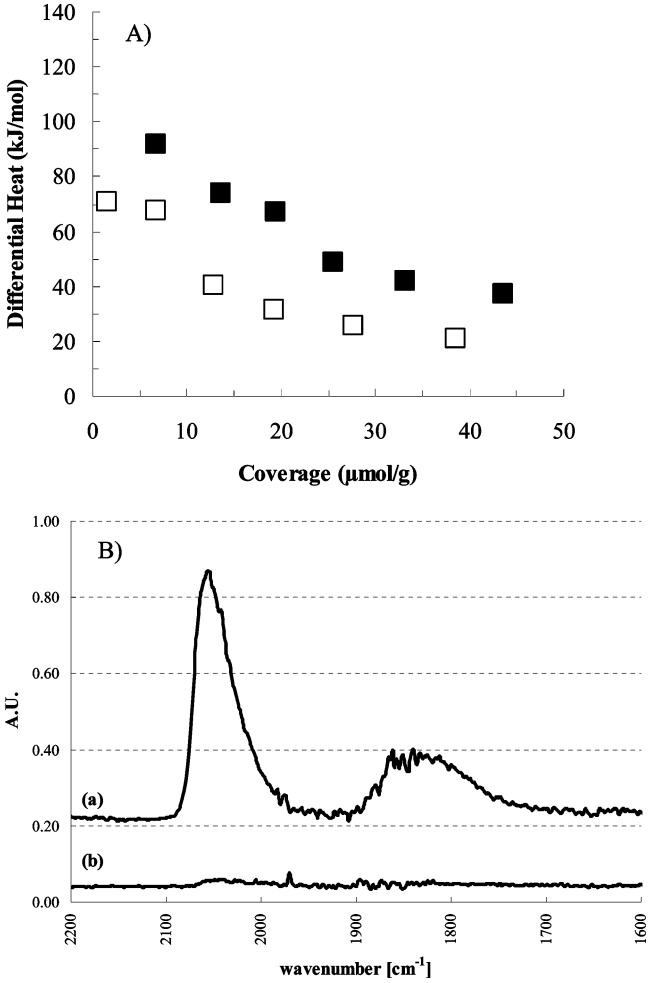

Figure 3. (A) Microcalorimetric adsorption of ethanol on capped silica supported catalysts at 300 K: (■) Pt and (□) Pt−Sn. (B) Infrared spectroscopy of ethanol adsorption on capped silica supported catalysts at 300 K: (a) Pt and (b) Pt−Sn.

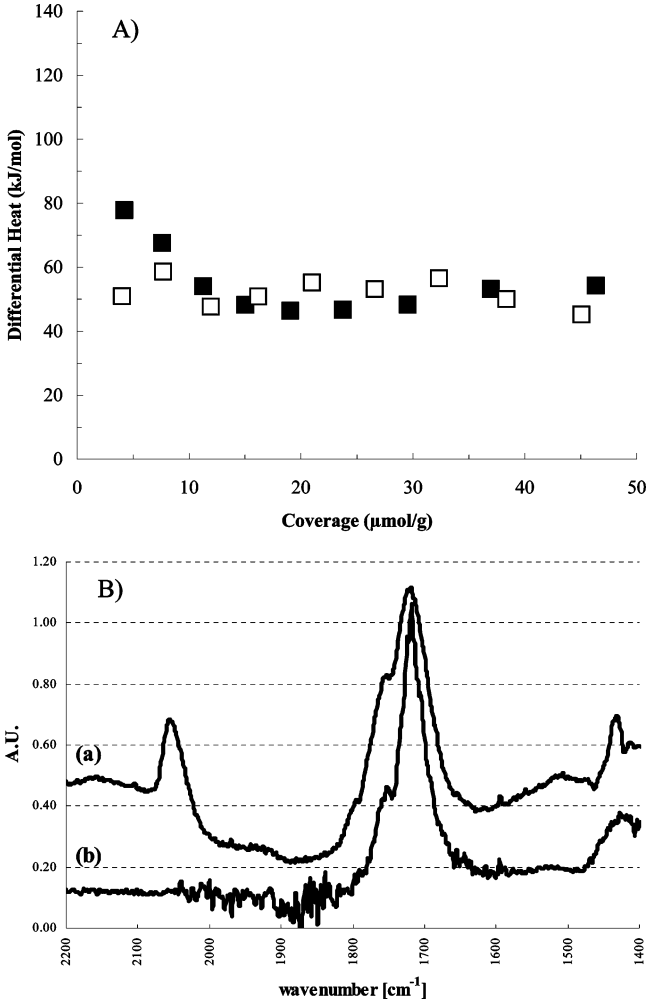

Figure 4. (A) Microcalorimetric adsorption of acetic acid on capped silica supported catalysts at 300 K: (■) Pt and (□) Pt−Sn. (B) Infrared spectroscopy of acetic acid adsorption on capped silica supported catalysts at 300 K: (a) Pt and (b) Pt−Sn.

CO (Figure 3B, spectrum (a)). The initial heat for ethanol adsorption on silica-supported PtSn is 70 kJ/mol (Figure 3A, open square symbols). Product gases are observed to desorb from the catalyst surface during these measurements, whereas adsorbed CO species are not formed from ethanol adsorption on Pt−Sn alloy catalysts (Figure 3B, spectrum (b)).

Figure 4A shows microcalorimetric data for the interaction of acetic acid with capped Pt and PtSn catalysts. The initial heat for acetic acid adsorption on Pt (solid square symbols) is 80 kJ/mol, slightly lower than the value for ethanol adsorption. These measurements were accompanied by the formation of product gases from acetic acid decomposition (dehydrogenation and C−C bond cleavage). In addition, exposure of Pt to acetic acid at these conditions lead to the appearance of an infrared band at 2060 cm^{-1}, corresponding to atop-adsorbed CO (Figure 4B, spectrum (a)) as well as formation of bands centered near 1720 and 1430 cm^{-1} corresponding to adsorbed acetic acid (carbonyl stretch) and acetate (CH_3COO) species, respectively. The initial heat for interaction of acetic acid with silica-supported Pt−Sn is approximately 55 kJ/mol (Figure 4A, open square symbols). In contrast to the behavior of Pt, residual gas pressure was not detected after acetic acid adsorption on the Pt−Sn catalyst, and IR bands from adsorbed CO were not present for the Pt−Sn catalysts (Figure 4B, spectrum (b)). Instead, IR bands were observed at 1720 and 1430 cm^{-1} for adsorbed acetic acid and acetate (CH_3COO) species, respectively.

(2) Reaction Kinetic Studies. Figure 5 shows the rates of production of various species from ethanol in a hydrogen-rich feed stream. The major products over Pt/SiO_2 are equimolar amounts of CO and CH_4 (activation energy of 93 kJ/mol), accompanied by acetaldehyde (activation energy of 51 kJ/mol) and ethane (activation energy of 49 kJ/mol). As tin is added to the catalyst, the production of ethane slows drastically, and methane and acetaldehyde production decrease. Accordingly, the activation barrier for ethane production increases to 54 kJ/mol over $PtSn_{0.8}/SiO_2$, while the barrier for methane and acetaldehyde production is essentially unchanged. Finally, C−O and C−C bond cleavage cease over the $PtSn_4$ catalyst, such that acetaldehyde becomes the major product with an increased barrier of about 65 kJ/mol. As suggested by Scheme 1(a), the conversion of ethanol begins with dehydrogenation to form acetaldehyde, and this reaction may take place through adsorbed ethoxy (CH_3CH_2O) or 1-hydroxyethyl (CH_3CHOH) intermediates. As depicted in Scheme 1b, acetaldehyde may decompose through C−C bond cleavage to form CO and CH_4, or it may decompose through C−O bond cleavage to form C_2H_6.

Rates of production of various species from acetic acid are shown in Figure 6, and several data for the conversion of ethanol are given for comparison. The conversion of acetic acid begins with dehydroxylation to form adsorbed acetyl (CH_3CO) species as suggested by Scheme 1(b). In a parallel reaction network, the acetyl (CH_3CO) species can decompose to form CH_4 and

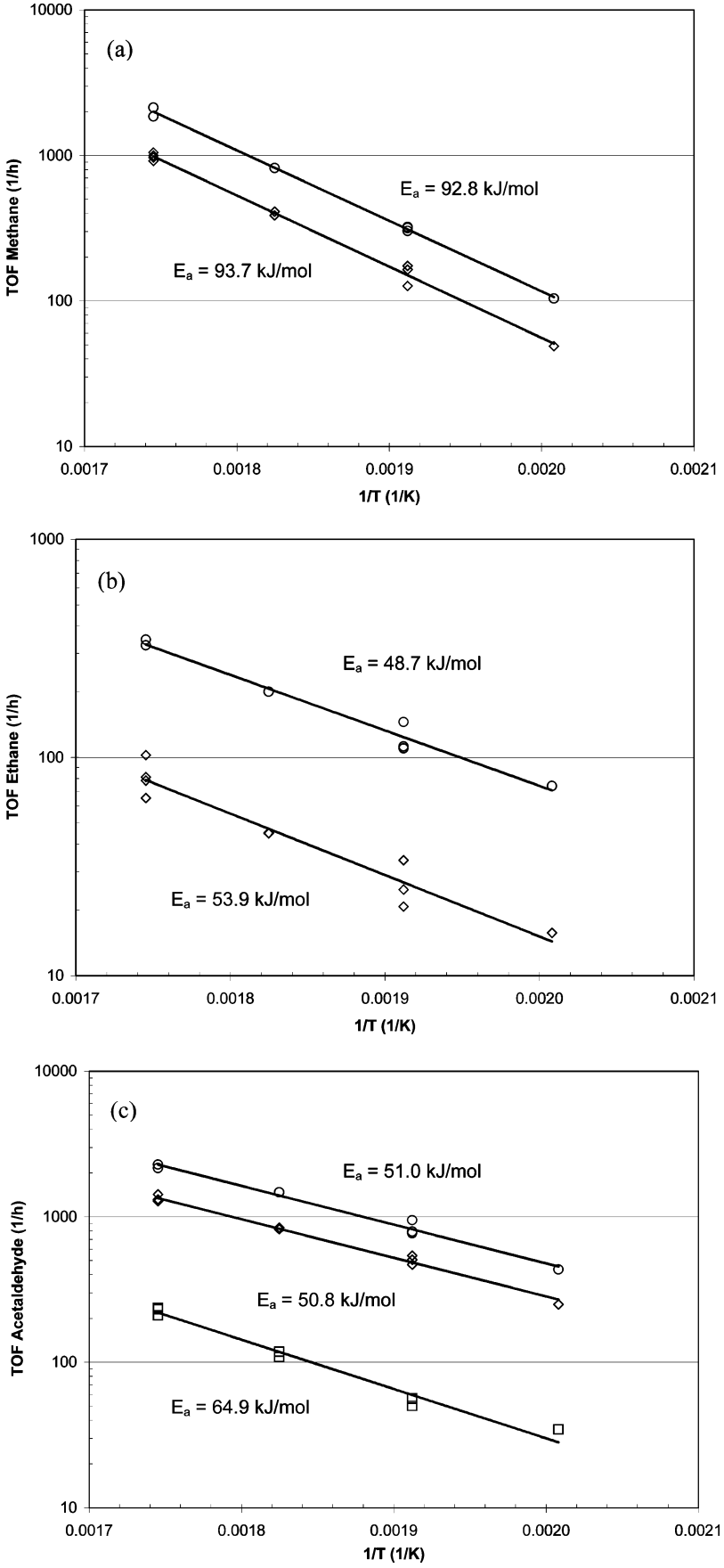

Figure 5. Reaction kinetics data for ethanol reactions on Pt/SiO_2 (circles); $PtSn_{0.8}/SiO_2$ (diamonds); and $PtSn_4/SiO_2$ (squares). Turnover frequency of (a) methane production, (b) ethane production, and (c) acetaldehyde production. Note: feed consists of 4.8 mol % oxygenate, 80 mol % H_2, and balance He.

TABLE 2: Electronic Energies (kJ/mol) from DFT Calculations for Surface Reactions on $Pt_3Sn(111)$[a] Relative to Gas-Phase Ethanol and Clean Slab(s)[c]

	surface reactions[a]				
intermediate (stoichiometry)	intermediate	C−O TS	C−O cleavage	C−C TS	C−C cleavage
ethanol (CH_3CH_2OH)	−29	(162)	32	(155)	23
ethoxy (CH_3CH_2O)	30	(236)	87	(194)	50
1-hydroxyethyl (CH_3CHOH)	−6	(206)	56	(190)	24
2-hydroxyethyl (CH_2CH_2OH)	11	(188)	24	(215)	46
acetaldehyde (CH_3CHO)	−26	(209)	110	(158)	−13
ethylene oxide (CH_2CH_2O)	12	(210)	78	(203)	72
1-hydroxyethylidene (CH_3COH)	−34	66	0	(172)	−13
hydroxyethylene (CH_2CHOH)	−38	(168)	25	(186)	46
2-hydroxyethylidene ($CHCH_2OH$)	13	(213)	25	(243)	18
acetyl (CH_3CO)	−86	153	54	62	−111
formylmethyl (CH_2CHO)	−42	(186)	80	(169)	9
($CHCH_2O$)	17	(238)	80	(233)	44
1-hydroxyvinyl (CH_2COH)	−39	(180)	35	(192)	9
2-hydroxyvinyl ($CHCHOH$)	−34	(162)	33	(214)	18
2-hydroxyethylidyne (CCH_2OH)	−18	(199)	35	(223)	99
ketene (CH_2CO)	−87	269	89	71	−89
formylmethylene ($CHCHO$)	−54	(165)	87	(184)	−19
(CCH_2O)	77	(304)	89	(294)	126
hydroxyacetylene ($CHCOH$)	−54	(180)	122	(204)	−19
hydroxyvinylidene ($CCHOH$)	−37	(195)	122	240	99
ketenyl ($CHCO$)	−100	(161)[b]	176	65	−117
formylmethylidyne ($CCHO$)	−33	(220)	176	(210)	62
hydroxyethynyl ($CCOH$)	48	(299)	247	(302)	62
(CCO)	−67	(219)[b]	301	(697)	−36

[a] Excess H adsorbs on a separate slab; bond cleavage products adsorb on separate slabs. [b] Predicted transition-state energies result in negative activation barriers. [c] H_2 heat of adsorption on $Pt_3Sn(111)$ is 103 kJ/mol. Values in parentheses are estimated from linear correlation plot (standard error = 78 kJ/mol).

SCHEME 1: Reaction Pathways: (a) Ethanol Dehydrogenation and (b) Ethanol, Acetaldehyde, and Acetic Acid Decomposition

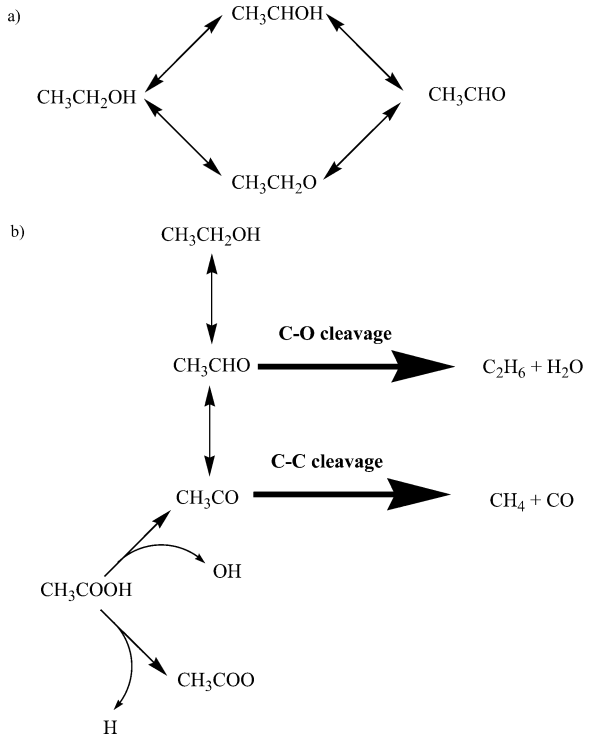

CO, or it can undergo hydrogenation to form acetaldehyde or ethanol. At temperatures between 473 and 598 K, acetic acid is converted to equal amounts of CH_4 and CO by C−C bond cleavage over Pt/SiO_2 catalysts. As tin is added to the Pt catalyst, the rate of C−C bond cleavage decreases dramatically (Figure 6(c)), while the rate of production of acetaldehyde increases (Figure 6(b)). Some of the acetaldehyde is converted to ethanol in the hydrogen-rich environment, and these oxygenates may undergo esterification reactions with acetic acid to form small amounts of ethyl acetate (Figure 6(f)). Formation of C_2H_6 by C−O bond cleavage (Figure 5(b) and 6(d)) is slower than C−C bond cleavage over Pt- and $PtSn/SiO_2$ catalysts, especially at high temperatures.

Figure 7 shows the reaction quotient for ethanol dehydrogenation, Q, given by

$$Q = \frac{P_{AcH} P_{H2}}{P_{EtOH}}$$

where P_{AcH}, P_{H2}, and P_{EtOH} are the partial pressures of acetaldehyde, hydrogen, and ethanol, respectively. The solid line corresponds to the calculated ethanol−acetaldehyde thermodynamic equilibrium as a function of temperature. It can be seen in Figure 7 that ethanol dehydrogenation is quasi-equilibrated over Pt and $PtSn_{0.8}/SiO_2$ catalysts, whereas this reaction does not reach equilibrium over $PtSn_4/SiO_2$. Figure 7 shows that at temperatures between 473 and 573 K the hydrogenation of acetaldehyde to form ethanol is acetaldehyde-rich over $PtSn_4/SiO_2$. Similarly, ethanol dehydrogenation to form acetaldehyde is ethanol-rich over $PtSn_4/SiO_2$, leading to the low apparent rate of acetaldehyde production from ethanol shown in Figures 5(c) and 6(b).

(3) Density Functional Theory Calculations. *C−H and O−H Bond Cleavage Reactions.* Electronic energy changes for the formation of various surface species by dehydrogenation of ethanol on $Pt_3Sn(111)$ are shown in Table 2. These energies are calculated with respect to gas-phase ethanol (and clean Pt_3Sn slabs) (θ = 1/4 ML), and the hydrogen atoms removed from ethanol to form these species are adsorbed on separate Pt_3Sn slabs.

Dehydrogenation of ethanol can proceed through ethoxy (CH_3CH_2O) and 1-hydroxyethyl (CH_3CHOH) intermediates via parallel pathways as shown in Scheme 1(a). The transition-state energies to form ethoxy (CH_3CH_2O) and 1-hydroxyethyl (CH_3CHOH) species on $Pt_3Sn(111)$ are 56 and 68 kJ/mol, respectively, relative to gas-phase ethanol. The initial dehydrogenation

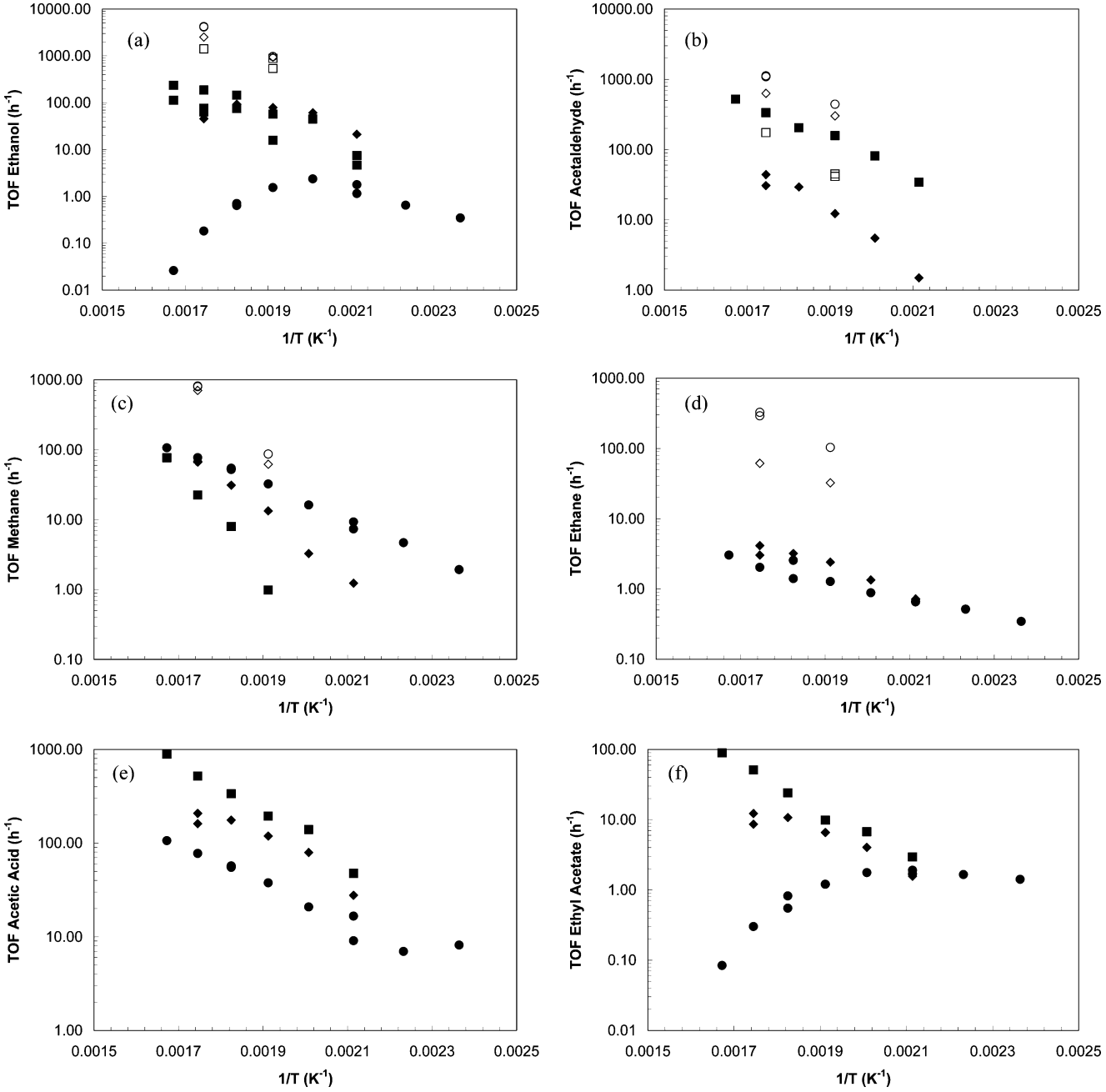

Figure 6. Reaction kinetics data for acetic acid (solid symbols) and ethanol (open symbols) reactions on Pt/SiO_2 (circles), $PtSn_{0.8}/SiO_2$ (diamonds), and $PtSn_4/SiO_2$ (squares). Turnover frequency of (a) ethanol consumption/production, (b) acetaldehyde production, (c) CH_4 production, (d) C_2H_6 production, (e) acetic acid consumption, and (f) ethyl acetate production. Note: feed consists of 2.5 mol % oxygenate, 80 mol % H_2, and 17.5 mol % He.

reactions have higher transition-state energies compared to subsequent dehydrogenation reactions. Therefore, the lowest energy pathway for acetaldehyde formation is via the ethoxy species on $Pt_3Sn(111)$.

On Pt(111), transition-state energies for ethanol dehydrogenation to form ethoxy (CH_3CH_2O) and 1-hydroxyethyl (CH_3CHOH) species are 51 and 44 kJ/mol, respectively, relative to gas-phase ethanol.[20] Subsequent dehydrogenation transition-state energies are lower. Thus, the lowest energy pathway for formation of acetaldehyde on Pt(111) is via the 1-hydroxyethyl (CH_3CHOH) species. Results from DFT studies for methanol dehydrogenation on Pt(111) have reported lower transition-state barriers to form hydroxymethyl intermediates compared to methoxy intermediates.[31]

C−O and C−C Bond Cleavage Reactions. In a previous study, we have identified various transition states for cleavage of C−O and C−C bonds in species derived from ethanol on Pt(111).[20] In that study we employed a strategy in which transition states were first identified for reactions that have favorable thermodynamics. A correlation was then developed for the energies of these transition states in terms of the energies of the corresponding final states, and this correlation was used to estimate the energies of transition states for other C−O and C−C bond cleavage reactions. We now employ the same strategy to study pathways for cleavage of C−O and C−C bonds on $Pt_3Sn(111)$.

To identify favorable surface intermediates for C−O and C−C bond cleavage, the energies of adsorption for all possible bond cleavage products were investigated on the $Pt_3Sn(111)$ surface. Changes in electronic energies corresponding to the formation of products by C−O and C−C bond cleavage are listed in Table 2. These results were then used to guide the

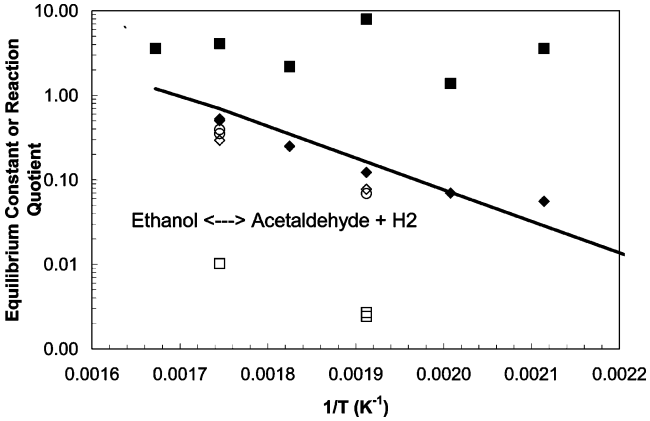

Figure 7. Ethanol and acetaldehyde reaction quotient and chemical equilibrium as a function of temperature. The solid line corresponds to the ethanol−acetaldehyde thermodynamic equilibrium, while the symbols correspond to data in Figure 6.

search for low-energy transition states. Accordingly, three and four routes for C−O and C−C bond cleavage, respectively, were investigated. Electronic energies corresponding to these transition states are listed in Tables 2.

The lowest energy transition state for C−O bond cleavage corresponds to the 1-hydroxyethylidene (CH_3COH) species. The energy of this transition-state energy for C−O bond cleavage is 66 kJ/mol. Products of this C−O bond cleavage reaction are ethylidyne (CH_3C) and hydroxyl (OH) species. These species adsorb on 3-fold hcp and bridge sites, respectively. The binding of hydroxyl (OH) species on the $Pt_3Sn(111)$ surface is relatively insensitive to the nature of the binding surface atom, with a difference between adsorption on Pt and Sn adsorption of only 8 kJ/mol. In addition, the hydroxyl species is the only species with a higher binding energy on $Pt_3Sn(111)$ compared to Pt(111) (the difference is 15 kJ/mol).

The lowest energy transition state for C−C bond cleavage corresponds to the acetyl (CH_3CO) species, and the energy of this transition state for C−C bond cleavage is 62 kJ/mol. The methyl (CH_3) and CO product species adsorb on atop and 3-fold hcp sites, respectively. Preferential adsorption of CO on 3-fold sites is in agreement with reported DFT studies, although experimental results indicate CO adsorption occurs on bridge and atop sites.[39]

Figure 8 shows a simplified potential energy diagram of the stabilities and reactivities of dehydrogenated species derived from ethanol on $Pt_3Sn(111)$. Views of adsorbed species and transition states are shown in the insets. We next address the energies of transition states for other C−O and C−C bond cleavage reactions. Since the energy of the transition state for C−O bond cleavage through 1-hydroxyethylidene (CH_3COH) species is only 66 kJ/mol, we can eliminate 14 other possible transition states for C−O bond cleavage in Table 2 as kinetically unimportant, since the energies of the products for these reactions are already higher than 66 kJ/mol compared to gaseous ethanol. Similarly, since the energy of the transition state for C−C bond cleavage through acetyl (CH_3CO) species is 62 kJ/mol, we can eliminate five other possible transition states for C−C bond cleavage in Table 2 as being kinetically unimportant. To address whether additional bond cleavage reactions through the remaining adsorbed species in Table 2 may be competitive with the most favorable pathways identified in Figure 8, we estimate the transition-state energies for these additional pathways from the energies of calculated transition states in Table 2. In this respect, we use a Brønsted−Evans−Polanyi type correlation to relate the transition-state energy of the products for an exothermic reaction. Accordingly, Figure 9 is a plot of transition-state energies versus the corresponding final state energies for the transition states of Table 2, where each surface reaction is defined in the exothermic direction. The predicted energies of these remaining transition states are listed in Table 2, from which it can be seen that none of these additional pathways is competitive with the most favorable pathways that we have already found, i.e., C−O bond cleavage through 1-hydroxyethylidene (CH_3COH) and C−C bond cleavage through acetyl (CH_3CO) species.

Finally, we compare the energies of the transition states for cleavage of the CH_3CO−OH bond in acetic acid. This reaction leads to the formation of adsorbed CH_3CO species that can lead to acetaldehyde or ethanol or can undergo further C−O or C−C bond cleavage reactions. The reaction in Scheme 1(b) shows acetic acid dehydroxylation, hydrogenation, and C−C and C−O bond cleavage reactions. The transition state for cleavage of the CH_3CO−OH bond in acetic acid on $Pt_3Sn(111)$ takes place over a Pt−Pt bridge site. The energy of this transition state is 73 kJ/mol relative to gas-phase acetic acid. For comparison, the energy of the transition state for acetic acid dissociation is 61 kJ/mol on Pt(111), and this reaction also occurs on a bridge site. The results from these calculations indicate that the transition-state energy for acetic acid dissociation on $Pt_3Sn(111)$ is only slightly higher (by 12 kJ/mol) than on Pt(111).

Discussion

The Mössbauer spectra of the present study show that the major phase of the silica-supported PtSn catalysts is a PtSn alloy, with small amounts of ionic Sn phases. After exposing the catalyst to reaction conditions, the PtSn phase for both catalysts remains intact, while the relative area of the Sn(IV) species increases and the relative area of the Sn(II) species decreases. While the chemical composition of species is not strictly proportional to the relative area in the Mössbauer spectra (because of differences in recoil-free fractions), it appears that the increase in the Sn(IV) species occurs from oxidation of the Sn(II) species, and these ionic Sn(II) and Sn(IV) species are likely associated with the silica support. Accordingly, the catalytically active phase of the $PtSn/SiO_2$ catalysts is most likely the Pt−Sn alloy. These results are consistent with those of Jerdev et al., who observed that model Sn/Pt(111) surfaces formed PtSn alloys which were twice as active as Pt(111) surfaces for hydrogenation of crotonaldehyde.[40] They also observed that oxidic Sn species were not stable under reaction conditions.

Results from reaction kinetics studies of the conversions of ethanol and acetic acid over PtSn-based catalysts compared to Pt-based catalysts indicate that the formation of decomposition products such as CO, CH_4, and C_2H_6 is suppressed by the presence of Sn. Importantly, the rates of ethanol dehydrogenation to acetaldehyde are comparable over PtSn- and Pt-based catalysts, and PtSn-based catalysts show high rates for the reduction of acetic acid to form ethanol. The results from these experimental studies thus indicate that (i) the rates of hydrogenation−dehydrogenation reactions are similar over PtSn- and Pt-based catalysts, (ii) the apparent rates of acetic acid reduction increase over PtSn-based catalysts, whereas (iii) the rates of C−O and C−C bond cleavage reactions in dehydrogenated species derived from ethanol are considerably lower on PtSn-based catalysts compared to Pt catalysts.

Brønsted−Evans−Polanyi type correlations for ethanol dehydrogenation reactions on $Pt_3Sn(111)$ and Pt(111) are shown in Figure 9. Linear fits for these results on $Pt_3Sn(111)$ and Pt(111) have slopes near unity and nearly equal intercepts.

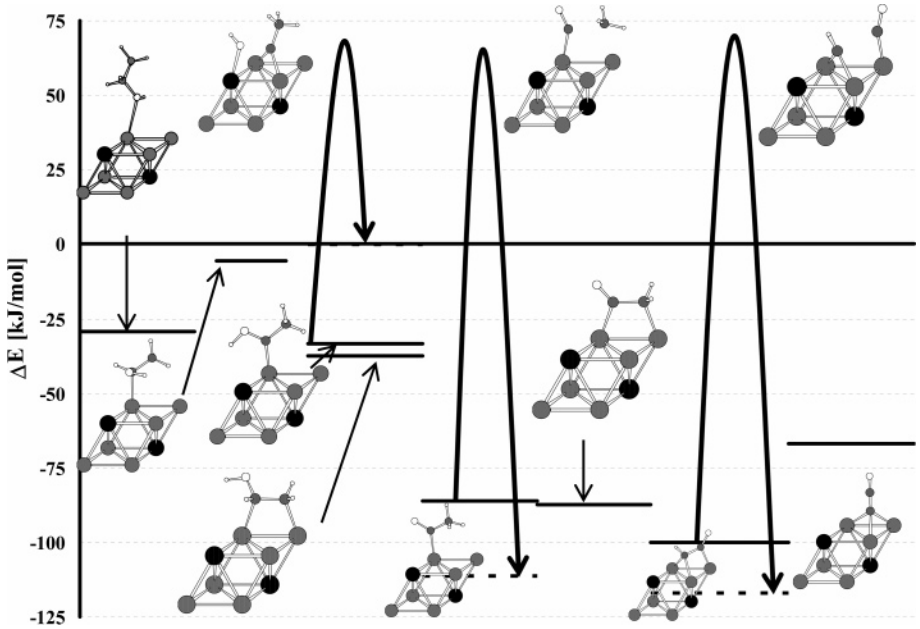

Figure 8. Potential energy diagram for ethanol reactions on $Pt_3Sn(111)$. The reference state is gas-phase ethanol and clean slab(s). Removed H atoms and bond cleavage products are each adsorbed on separate slabs. Solid curves represent bond cleavage reactions. Insets show views of stable and transition-state species. The large gray circles represent Pt atoms, large black circles represent Sn atoms, gray medium circles represent C atoms, white medium circles represent O atoms, and small white circles represent H atoms.

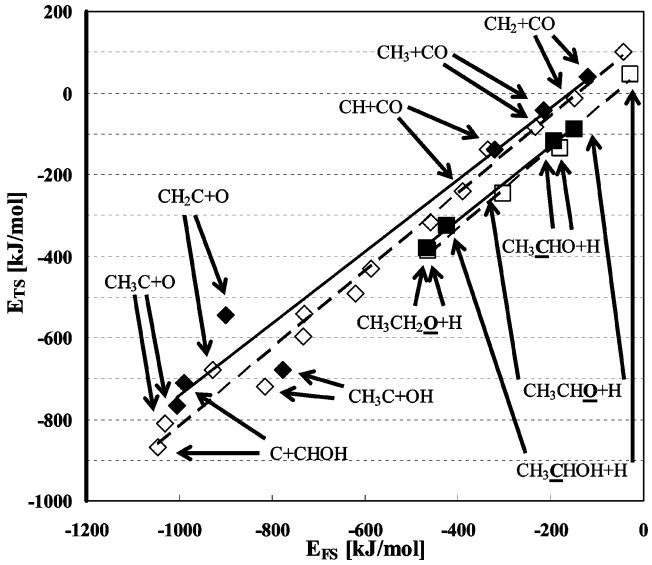

Figure 9. Correlation plot for C−O (■), C−C (■), and H (◆) bond cleavage reactions on $Pt_3Sn(111)$. Note: Pt(111) results are shown as open symbols and dashed lines. Final state (E_{FS}) and transition-state (E_{TS}) energies are relative to initial state gas-phase energies. Surface reactions are defined in the exothermic direction. The C−O and C−C bond cleavage linear regression equation is E_{TS} [kJ/mol] = $0.88E_{FS}$ [kJ/mol] + 138 kJ/mol, and the standard error is 78 kJ/mol. The C−H and O−H bond cleavage linear regression equation is E_{TS} [kJ/mol] = $0.91E_{FS}$ [kJ/mol] + 53 kJ/mol, and the standard error is 9 kJ/mol.

Pathways for ethanol dehydrogenation reactions forming acetaldehyde are shown in Scheme 1(a). In this subset of reaction intermediates, the 1-hydroxyethyl species is the only species that binds to the surface through a C atom, and its binding energy is weakened most on $Pt_3Sn(111)$. In particular, the binding energies of 1-hydroxyethyl (CH_3CHOH) species are equal to 128 and 159 kJ/mol on $Pt_3Sn(111)$ and Pt(111), respectively. The binding energies of ethanol, ethoxy, and acetaldehyde species are weakened by less than 6 kJ/mol on $Pt_3Sn(111)$. These effects of Sn on the binding energies of surface species lead to changes in the nature of the reaction pathway for initial dehydrogenation of ethanol, such that ethanol dehydrogenation takes place through 1-hydroxyethyl (CH_3CHOH) species on Pt(111) and through ethoxy species on $Pt_3Sn(111)$. However, the energy for the most favorable transition state for ethanol dehydrogenation on Pt(111) is only 12 kJ/mol higher than the most favorable transition state for ethanol dehydrogenation on $Pt_3Sn(111)$. This finding is consistent with our experimental result that PtSn-based catalysts are active for hydrogenation−dehydrogenation conversions between acetaldehyde and ethanol.

Results from DFT calculations for C−O and C−C bond cleavage transition states from ethanol-derived species on $Pt_3Sn(111)$ and Pt(111) are consistent with our experimental finding that PtSn catalysts exhibit lower rates of ethanol C−O bond cleavage reaction rates (forming C_2H_6) compared to Pt catalysts. The catalytic activity differences between $Pt_3Sn(111)$ and Pt(111) may be interpreted using the Brønsted−Evans−Polanyi type correlations in Figure 9. In all cases, final state energies on $Pt_3Sn(111)$ are higher compared to Pt(111), and the transition-state energies are thus higher on $Pt_3Sn(111)$. For example, the transition-state energy for C−O bond cleavage in 1-hydroxyethylidene (CH_3COH) on $Pt_3Sn(111)$ is 66 kJ/mol relative to gas-phase ethanol, and this transition state has the lowest energy for C−O bond cleavage reactions in ethanol-derived intermediates. This value is 24 kJ/mol higher compared to Pt(111). The energy of 1-hydroxyethylidene (CH_3COH) species is 39 kJ/mol larger on $Pt_3Sn(111)$ compared to Pt(111), respectively, relative to the common reference state (gas-phase ethylidyne (CH_3C) and hydroxyl (OH) species). Thus, the higher final state energy (E_{FS}) on $Pt_3Sn(111)$ compared to Pt(111) correlates to the increased transition-state energy for C−O bond cleavage in 1-hydroxyethylidene (CH_3COH).

The energy of the transition state for C−C bond cleavage in ketenyl (CHCO) species on $Pt_3Sn(111)$ is 65 kJ/mol relative to gas-phase ethanol. This value is 61 kJ/mol higher compared to C−C bond cleavage in ketenyl (CHCO) species on Pt(111). This large increase in the energy of the transition state may be attributed to the energetic difference for adsorption of meth-

ylidyne (CH) species on the different surfaces. The corresponding energies of methylidyne (CH) and CO are 67 and 3 kJ/mol larger on $Pt_3Sn(111)$ compared to Pt(111), relative to the common reference state (gas-phase ketenyl (CHCO) species). Thus, the final state energy (E_{FS}) is 70 kJ/mol higher on $Pt_3Sn(111)$ compared to Pt(111), and this difference correlates with the increased transition-state energy for ketenyl (CHCO) C−C bond cleavage.

Although the lowest energy transition state for C−C bond cleavage on Pt(111) involves the ketenyl (CHCO) species, the lowest energy transition state on $Pt_3Sn(111)$ is through the acetyl (CH_3CO) species. The energy of this transition state on $Pt_3Sn(111)$ is 62 kJ/mol relative to gas-phase ethanol, which is 17 kJ/mol higher compared to the transition-state energy for C−C bond cleavage in acetyl (CH_3CO) species on Pt(111). The corresponding energies for methyl (CH_3) and CO species are 16 and 3 kJ/mol higher on $Pt_3Sn(111)$ compared to Pt(111), relative to the common reference state (gas-phase acetyl (CH_3CO) species). Thus, the final state energy (E_{FS}) is 19 kJ/mol higher on $Pt_3Sn(111)$ compared to Pt(111), and this difference correlates with the increased transition-state energy for acetyl (CH_3CO) C−C bond cleavage.

Results from DFT calculations for CH_3CO-OH bond cleavage in acetic acid indicate that the energies of the transition states on $Pt_3Sn(111)$ and Pt(111) are similar. Specifically, the energy of the transition state for CH_3CO-OH bond cleavage in acetic acid on $Pt_3Sn(111)$ is 73 kJ/mol relative to gas-phase acetic acid, and this value is only 12 kJ/mol higher compared to the transition-state energy on Pt(111). This results suggests that acetic acid reactivity should be similar over Pt(111) and $Pt_3Sn(111)$ with respect to the first step in its decomposition.

Acetaldehyde and ethanol species formed from acetic acid may undergo C−C and C−O bond cleavage. The results from our experimental studies show that Pt catalysts are selective for C−C bond cleavage (CH_4 and CO) compared to C−O bond cleavage (C_2H_6). In agreement with this observation, results from our DFT calculations indicate that the lowest energy transition states for C−C bond cleavage on Pt(111) has an energy of 4 kJ/mol, and this value is lower than the value of 42 kJ/mol for the corresponding transition state for C−O bond cleavage. The energies of these transition states for C−C and C−O bond cleavage increase by 25−60 kJ/mol on $Pt_3Sn(111)$, and this change is consistent with the experimental result that PtSn-based catalysts are selective for acetic acid conversion to acetaldehyde and ethanol rather than to alkanes.

An interesting experimental observation of the present study is that the rate of acetic acid conversion is higher for PtSn-based catalysts compared to Pt catalysts. In contrast, the results from DFT calculations indicate that the transition state energy for CH_3CO-OH bond cleavage is higher on $Pt_3Sn(111)$ compared to Pt(111), i.e., 73 compared to 61 kJ/mol. Thus, the higher reactivity of the PtSn-based catalysts may be explained by observation that acetic acid decomposition on Pt catalysts leads to formation of CO, which adsorbs strongly on Pt and blocks surface sites for acetic acid conversion. Catalytically active sites on PtSn catalysts are not covered with CO because C−C bond cleavage reactions are inhibited on PtSn catalysts.

The experimental results in Figures 5 and 6 indicate that the rate of ethanol consumption is significantly higher than that of acetic acid conversion over Pt and PtSn-based catalysts. In agreement with this observation, results from DFT calculations indicate that the transition-state energies for acetic acid dehydroxylation (CH_3CO-OH bond cleavage) are higher by 17 kJ/mol compared to the transition-state energies for ethanol dehydrogenation (CH_3CH_2O-H bond cleavage) on Pt(111) and $Pt_3Sn(111)$.

It can be seen in Figure 6(f) that addition of Sn to Pt dramatically increases the rate of formation of ethyl acetate from acetic acid conversion. In fact, ethyl acetate is only observed in large quantities when acetic acid is present in the feed. Thus, ethyl acetate appears to be formed from surface species derived from ethanol and acetic acid, such as from ethoxy (CH_3CH_2O) and acetyl (CH_3CO) species. While we have not conducted DFT calculations for such reactions, we expect that the transition state for reaction of acetyl (CH_3CO) with ethoxy (CH_3CH_2O) species would be similar to that for reaction with hydroxyl (OH) species. Therefore, we suggest that the addition of Sn to Pt has a smaller effect on the transition state for the esterification reaction (i.e., an effect of 12 kJ/mol, based on our results for the reaction of acetyl (CH_3CO) species with hydroxyl (OH) groups) than the effect of Sn on the transition states for C−C and C−O bond cleavage in species derived from ethanol (which are significantly destabilized by addition of Sn). In this way, addition of Sn to Pt allows ethoxy (CH_3CH_2O) species to react with acetyl (CH_3CO) species (to form ethyl acetate) by suppressing the decomposition of ethoxy (CH_3CH_2O) species through C−C and C−O bond cleavage reactions (leading primarily to the formation of methane and CO).

The results from our microcalorimetric and infrared spectroscopic measurements of the interactions of ethanol and acetic acid with Pt and PtSn catalysts are in agreement with the above finding that Sn suppresses the rate of C−C bond cleavage in these oxygenated hydrocarbons. The initial heat for ethanol adsorption on silica supported Pt is 95 kJ/mol, gas evolution (e.g., hydrogen) is measured, and infrared spectroscopic experiments show the formation of adsorbed CO. In contrast, the initial heat on PtSn is 70 kJ/mol, adsorbed CO was not detected, and residual gas was detected in this case. To interpret these observations, we use results from our DFT calculations. Table 3 shows DFT-calculated energy changes to form adsorbed CO from C−C bond cleavage reactions in four ethanol-derived intermediates. Only one entry (ketenyl (CHCO)) is considerably more exothermic than 100 kJ/mol, leading to the following overall reaction on Pt(111):

$$CH_3CH_2OH(g) \rightarrow CH(a) + CO(a) + 5H(a) \qquad \Delta E = -144 \text{ kJ/mol}$$

The DFT-calculated energy change for desorption of H_2 from Pt is 86 kJ/mol. The heat for dihydrogen dissociative adsorption is coverage dependent and decreases with increasing coverage, such that the heat for hydrogen desorption from Pt catalysts is approximately 50 kJ/mol at high coverage.[35] Thus, the microcalorimetric value of 95 kJ/mol for the heat of interaction of ethanol with Pt is most likely caused by the dissociation of ketenyl species, accompanied by the recombination of some of the adsorbed H-atoms to form gaseous H_2. For the case of ethanol adsorption on PtSn, results from DFT calculations for $Pt_3Sn(111)$ indicate that several reactions are consistent with the experimental findings:

$$CH_3CH_2OH(g) \rightarrow CH_3CO(a) + 3H(a) \quad \Delta E = -86 \text{ kJ/mol}$$

$$CH_3CH_2OH(g) \rightarrow CH_2CO(a) + 4H(a) \quad \Delta E = -87 \text{ kJ/mol}$$

$$CH_3CH_2OH(g) \rightarrow CHCO(a) + 5H(a) \quad \Delta E = -100 \text{ kJ/mol}$$

TABLE 3: Electronic Energies (kJ/mol) from DFT Calculations for Surface Reactions on Pt(111) and $Pt_3Sn(111)$ Relative to Gas-Phase Ethanol and Clean Slab(s)[a]

	Pt(111)		$Pt_3Sn(111)$	
intermediate (stoichiometry)	intermediate	C−C cleavage	intermediate	C−C cleavage
ethanol (CH_3CH_2OH)	−27	17	−29	23
ethoxy (CH_3CH_2O)	38	32	30	50
1-hydroxyethyl (CH_3CHOH)	−28	−12	−6	24
2-hydroxyethyl (CH_2CH_2OH)	−1	37	11	46
acetaldehyde (CH_3CHO)	−4	−31	−26	−13
ethylene oxide (CH_2CH_2O)	14	52	12	72
1-hydroxyethylidene (CH_3COH)	−55	−78	−34	−13
hydroxyethylene (CH_2CHOH)	−44	8	−38	46
2-hydroxyethylidene ($CHCH_2OH$)	1	−23	13	18
acetyl (CH_3CO)	−84	**−104**	−86	**−111**
formylmethyl (CH_2CHO)	−30	−11	−42	9
($CHCH_2O$)	30	−9	17	44
1-hydroxyvinyl (CH_2COH)	−70	−58	−39	9
2-hydroxyvinyl ($CHCHOH$)	−48	−53	−34	18
2-hydroxyethylidyne (CCH_2OH)	−67	47	−18	99
ketene (CH_2CO)	−82	**−84**	−87	**−89**
formylmethylene ($CHCHO$)	−34	−72	−54	−19
(CCH_2O)	83	62	77	126
hydroxyacetylene ($CHCOH$)	−63	−119	−54	−19
hydroxyvinylidene ($CCHOH$)	−61	18	−37	99
ketenyl ($CHCO$)	−88	**−144**	−100	**−117**
formylmethylidyne ($CCHO$)	−42	−1	−33	62
hydroxyethynyl ($CCOH$)	37	−48	48	62
(CCO)	−53	**−74**	−67	**−36**

[a] Excess H adsorbs on a separate slab; bond cleavage products adsorb on separate slabs. Corresponding H_2 heats of adsorption are 86 and 103 kJ/mol. Values in bold correspond to cleavage reactions which form CO.

TABLE 4: Electronic Energies (kJ/mol) from DFT Calculations for Surface Reactions on Pt(111) and $Pt_3Sn(111)$ Relative to Gas-Phase Acetic Acid and Clean Slab(s)[a]

	Pt(111)		$Pt_3Sn(111)$	
intermediate (stoichiometry)	intermediate	C−C cleavage	intermediate	C−C cleavage
acetic acid (CH_3COOH)	−35		−34	
acetate (CH_3COO)	−121		−77	
acetyl (CH_3CO)	55	**35**	63	**38**
formylmethyl (CH_2CHO)	109	128	107	158
($CHCH_2O$)	179	130	166	193
1-hydroxyvinyl (CH_2COH)	69	81	110	158
2-hydroxyvinyl ($CHCHOH$)	91	86	115	167
2-hydroxyethylidyne (CCH_2OH)	72	186	131	248
ketene (CH_2CO)	57	**55**	62	**60**
formylmethylene ($CHCHO$)	105	67	95	130
(CCH_2O)	222	201	226	275
hydroxyacetylene ($CHCOH$)	76	20	95	130
hydroxyvinylidene ($CCHOH$)	78	157	112	248
ketenyl ($CHCO$)	51	**−5**	49	**32**
formylmethylidyne ($CCHO$)	97	138	116	211
hydroxyethynyl ($CCOH$)	176	91	197	211
(CCO)	86	**65**	82	**113**

[a] Excess hydroxyl (OH) and H adsorb on a separate slabs; bond cleavage products adsorb on separate slabs. Corresponding H_2 heats of adsorption are 86 and 103 kJ/mol. Values in bold correspond to cleavage reactions which form CO.

Importantly, in these cases cleavage of the C−C bond does not occur.

Microcalorimetric data for acetic acid adsorption on silica supported Pt indicate that the initial heat is 80 kJ/mol, and residual gas pressure is measured. Infrared spectroscopic experiments for acetic acid adsorption at the same temperature show the formation of adsorbed CO and acetate species. In contrast, the initial heat for acetic acid adsorption on PtSn is measured to be 55 kJ/mol, evolution of residual gas was not detected, and infrared spectroscopic experiments show only adsorbed acetate (CH_3COO) species and acetic acid. To interpret these observations, we use again results from our DFT calculations. Electronic energy changes for formation of acetic acid derived species are shown in Table 4. Three reactions for acetic acid adsorption and decomposition in Table 4 are exothermic for Pt(111):

$$CH_3COOH(g) \rightarrow CH_3COOH(a) \quad \Delta E = -35 \text{ kJ/mol}$$

$$CH_3COOH(g) \rightarrow CH(a) + CO(a) + OH(a) + 2H(a) \quad \Delta E = -5 \text{ kJ/mol}$$

$$CH_3COOH(g) \rightarrow CH_3COO(a) + H(a) \quad \Delta E = -121 \text{ kJ/mol}$$

Two reactions for acetic acid adsorption and dissociation in Table 4 are exothermic on $Pt_3Sn(111)$:

$$CH_3COOH(g) \rightarrow CH_3COOH(a) \quad \Delta E = -34 \text{ kJ/mol}$$

$$CH_3COOH(g) \rightarrow CH_3COO(a) + H(a) \quad \Delta E = -77 \text{ kJ/mol}$$

Formation of the acetate surface species is the most exothermic process on Pt(111) and $Pt_3Sn(111)$, and it appears that the microcalorimetric experiments may be dominated by this exothermic acetic acid dehydrogenation reaction.

Conclusions

In situ ^{119}Sn Mossbauer spectroscopy and microcalorimetric measurements of CO adsorption on silica-supported Pt−Sn catalysts indicate that these materials are comprised primarily of a Pt−Sn alloy phase before and after reaction kinetics studies of ethanol and acetic acid conversion in the presence of H_2. Electronic structure calculations employing periodic, self-consistent DFT were used to study the relative stabilities of various species derived from ethanol and acetic acid on Pt_3Sn-(111), and these results are compared with the behavior on Pt-(111). The lowest energy transition states for C−O and C−C bond cleavage on $Pt_3Sn(111)$ involve reactions of adsorbed 1-hydroxyethylidene (CH_3COH) and acetyl (CH_3CO) species, respectively. The energies of these transition state on Pt_3Sn-(111) are 25−60 kJ/mol higher compared to Pt(111), indicating that C−O and C−C bond cleavage reactions are inhibited on $Pt_3Sn(111)$. In contrast, energies of transition states for dehydrogenation−hydrogenation reactions increase by only 5−10 kJ/mol on $Pt_3Sn(111)$ compared to Pt(111). These results are in agreement with experimental results which show that the rates of hydrogenation−dehydrogenation reactions between ethanol and acetaldehyde are fast on PtSn-based catalysts as well as on Pt catalysts, whereas ethanol decomposition reactions leading to CO, CH_4, and C_2H_6 and involving C−C and C−O bond cleavage are inhibited by the presence of Sn. Results from DFT calculations also show that the transition-state energy for cleavage of the CH_3CO−OH bond in acetic acid increases by only 12 kJ/mol on $Pt_3Sn(111)$ compared to Pt(111). This prediction is consistent with the experimental observation that PtSn-based catalysts are selective for conversion of acetic acid to form acetaldehyde and ethanol, whereas Pt catalysts completely decompose acetic acid to CO, CH_4, and C_2H_6. A Brønsted−Evans−Polanyi type correlation has been developed to predict the transition-state energy for surface reactions in the conversion of these oxygenates based on the final state energy of the products.

Results from microcalorimetric and infrared spectroscopic measurements of the interactions of ethanol and acetic acid with Pt and PtSn catalysts are in agreement with our finding that Sn suppresses the rate of C−C bond cleavage in these oxygenated hydrocarbons. In particular, the presence of Sn leads to a decrease in the initial heat of interaction of these reactive molecules with silica-supported Pt catalysts at 300 K as well as the elimination of decomposition reactions leading to the presence of adsorbed CO. It is noteworthy that these microcalorimetric and infrared spectroscopic measurements for ethanol and acetic acid on Pt-based catalysts were achieved by "capping" the support by silylation, thereby minimizing the interaction of these oxygenated hydrocarbons with silanol groups of the support.

Acknowledgment. Rafael Alcalá acknowledges a Ford Predoctoral Fellowship from the National Research Council. In addition, we acknowledge funding from the National Science Foundation. We wish to thank Manos Mavrikakis for valuable discussions regarding DFT calculations and Paul Nealey for discussions regarding capping of silica.

References and Notes

(1) Cortright, R. D.; Sanchez-Castillo, M.; Dumesic, J. A. *Appl. Catal. B* **2002**, *39*, 353.
(2) Zhang, Z. G.; Jackson, J. E.; Miller, D. J. *Appl. Catal. A* **2001**, *219*, 89.
(3) Zhang, Z. G.; Jackson, J. E.; Miller, D. J. *Ind. Eng. Chem. Res.* **2002**, *41*, 691.
(4) Mao, B. W.; Cai, Z. Z.; Huang, M. Y.; Jiang, Y. Y. *Polym. Adv. Technol.* **2003**, *14*, 278.
(5) Anderson, R.; Griffin, K.; Johnston, P.; Alsters, P. L. *Adv. Synth. Catal.* **2003**, *345*, 517.
(6) Ji, H. B.; Qian, Y. *Chin. Chem. Lett.* **2003**, *14*, 615.
(7) Pillai, U. R.; Sahle-Demessie, E. *J. Catal.* **2002**, *211*, 434.
(8) Martin, S. E.; Suarez, D. F. *Tetrahedron Lett.* **2002**, *43*, 4475.
(9) Morales-Morales, D.; Redon, R.; Wang, Z. H.; Lee, D. W.; Yung, C.; Magnuson, K.; Jensen, C. M. *Can. J. Chem.* **2001**, *79*, 823.
(10) Dijksman, A.; Marino-Gonzalez, A.; Payeras, A. M. I.; Arends, I.; Sheldon, R. A. *J. Am. Chem. Soc.* **2001**, *123*, 6826.
(11) Baldi, M.; Milella, F.; Ramis, G.; Escribano, V. S.; Busca, G. *Appl. Catal. A* **1998**, *166*, 75.
(12) Mohanazadeh, F.; Ghamsari, S. *React. Funct. Polym.* **1996**, *29*, 193.
(13) Hill, J. M.; Cortright, R. D.; Dumesic, J. A. *Appl. Catal. A* **1998**, *168*, 9.
(14) Cortright, R. D.; Hill, J. M.; Dumesic, J. A. *Catal. Today* **2000**, *55*, 213.
(15) Bednarova, L.; Lyman, C. E.; Rytter, E.; Holmen, A. *J. Catal.* **2002**, *211*, 335.
(16) Larese, C.; Campos-Martin, J. M.; Calvino, J. J.; Blanco, G.; Fierro, J. L. G.; Kang, Z. C. *J. Catal.* **2002**, *208*, 467.
(17) Stagg, S. M.; Querini, C. A.; Alvarez, W. E.; Resasco, D. E. *J. Catal.* **1997**, *168*, 75.
(18) Llorca, J.; Homs, N.; Fierro, J. L. G.; Sales, J.; de la Piscina, P. R. *J. Catal.* **1997**, *166*, 44.
(19) Panja, C.; Saliba, N. A.; Koel, B. E. *Catal. Lett.* **2000**, *68*, 175.
(20) Alcala, R.; Mavrikakis, M.; Dumesic, J. A. *J. Catal.* **2003**, *218*, 178.
(21) Gursahani, K. I.; Alcala, R.; Cortright, R. D.; Dumesic, J. A. *Appl. Catal. A* **2001**, *222*, 369.
(22) Toba, M.; Tanaka, S.; Niwa, S.; Mizukami, F.; Koppany, Z.; Guczi, L.; Cheah, K. Y.; Tang, T. S. *Appl. Catal. A* **1999**, *189*, 243.
(23) Watwe, R. M.; Cortright, R. D.; Mavrikakis, M.; Norskov, J. K.; Dumesic, J. A. *J. Chem. Phys.* **2001**, *114*, 4663.
(24) Hammer, B.; Hansen, L. B.; Norskov, J. K. *Phys. Rev. B: Condens. Matter* **1999**, *59*, 7413.
(25) Vanderbilt, D. *Phys. Rev. B: Condens. Matter* **1990**, *41*, 7892.
(26) White, J. A.; Bird, D. M. *Phys. Rev. B: Condens. Matter* **1994**, *50*, 4954.
(27) Perdew, J. P.; Chevary, J. A.; Vosko, S. H.; Jackson, K. A.; Pederson, M. R.; Singh, D. J.; Fiolhais, C. *Phys. Rev. B: Condens. Matter* **1992**, *46*, 6671.
(28) Kresse, G.; Furthmuller, J. *Comput. Mater. Sci.* **1996**, *6*, 15.
(29) Watwe, R. M.; Cortright, R. D.; Norskov, J. K.; Dumesic, J. A. *J. Phys. Chem. B* **2000**, *104*, 2299.
(30) Alavi, A.; Hu, P. J.; Deutsch, T.; Silvestrelli, P. L.; Hutter, J. *Phys. Rev. Lett.* **1998**, *80*, 3650.
(31) Greeley, J.; Mavrikakis, M. *J. Am. Chem. Soc.* **2002**, *124*, 7193.
(32) Mills, G.; Jonsson, H.; Schenter, G. K. *Surf. Sci.* **1995**, *324*, 305.
(33) Henkelman, G.; Uberuaga, B. P.; Jonsson, H. *J. Chem. Phys.* **2000**, *113*, 9901.
(34) Henkelman, G.; Jonsson, H. *J. Chem. Phys.* **2000**, *113*, 9978.
(35) Shen, J. Y.; Hill, J. M.; Watwe, R. M.; Spiewak, B. E.; Dumesic, J. A. *J. Phys. Chem. B* **1999**, *103*, 3923.
(36) Carlos-Cuellar, S.; Li, P.; Christensen, A. P.; Krueger, B. J.; Burrichter, C.; Grassian, V. H. *J. Phys. Chem. A* **2003**, *107*, 4250.
(37) Santiago, M. A. N.; Sanchez-Castillo, M. A.; Cortright, R. D.; Dumesic, J. A. *J. Catal.* **2000**, *193*, 16.
(38) Margitfalvi, J. L.; Vanko, G.; Borbath, I.; Tompos, A.; Vertes, A. *J. Catal.* **2000**, *190*, 474.
(39) Feibelman, P. J.; Hammer, B.; Norskov, J. K.; Wagner, F.; Scheffler, M.; Stumpf, R.; Watwe, R.; Dumesic, J. *J. Phys. Chem. B* **2001**, *105*, 4018.
(40) Jerdev, D. I.; Olivas, A.; Koel, B. E. *J. Catal.* **2002**, *205*, 278.